

Spectroscopy

J. Synchrotron Rad. (1998), **5**, 989–991

XAFS and X-MCD spectroscopies with undulator gap scan

Andrei Rogalev,* Vincent Gotte, José Goulon, Christophe Gauthier, Joel Chavanne and Pascal Elleaume

European Synchrotron Radiation Facility, BP 220, F-38043 Grenoble CEDEX, France. E-mail: rogalev@esrf.fr

(Received 4 August 1997; accepted 27 October 1997)

The first experimental applications of the undulator gap-scan technique in X-ray absorption spectroscopy are reported. The key advantage of this method is that during EXAFS scans the undulator is permanently tuned to the maximum of its emission peak in order to maximize the photon statistics. In X-MCD or spin-polarized EXAFS studies with a helical undulator of the Helios type, the polarization rate can also be kept almost constant over a wide energy range.

Keywords: EXAFS; X-MCD; spin-polarized EXAFS; undulator sources.

1. Introduction

Undulator sources are very attractive for X-ray absorption spectroscopy because they offer an unprecedented spectral brilliance together with the possibility to minimize the heat load on the optics. Unfortunately, the spectral bandwidth of odd harmonics, which are most intense, may be large enough to cover the XANES region but is much too narrow to record a full EXAFS spectrum which extends over 1000–1500 eV. Moreover, since the photon flux varies dramatically when the monochromator is scanned across the undulator peak, the dynamic range of the detection system has to be large. Tapering the undulator gap results in a broadening of the spectral distribution but at the expense of a reduced source brilliance and a lower peak intensity: this was the strategy retained for the ESRF beamline ID24 (Hagelstein *et al.*, 1997). Alternatively, one may exploit even harmonics which exhibit a much wider bandwidth but again a lower peak intensity. A far better option is to move the undulator gap (or the half-gaps of a helical undulator) so that the energy of the X-ray monochromator always matches the maximum of the undulator peak. This technique, hereafter called ‘undulator gap scan’, is most attractive since it preserves the undulator brightness and keeps the intensity of the incoming beam almost constant over the whole EXAFS scan. Whenever a helical undulator is used, this technique offers the valuable advantage of also keeping the polarization state of the X-ray beam constant over a wide energy range.

The aim of this paper is to establish the practicability of the undulator gap-scan technique which is now routinely used at the ESRF ID12A beamline. Two examples were selected to illustrate the merits of this technique in X-ray absorption spectroscopies: the first concerns an EXAFS study of [d,l]

cystine at the sulfur *K*-edge; the second concerns spin-polarized XAFS spectra of EuS recorded at the Eu $L_{II,III}$ -edges in the ferromagnetic phase. A major concern in these experiments is the stability of the electron beam in the machine: the case of high-energy machines, such as ESRF, APS or SPring-8, is most favourable since the sensitivity of a machine to external perturbations scales as E^{-2} , where E is the electron beam energy. Considerable efforts have been made (*e.g.* with proper magnetic shimming of all insertion devices) to minimize such instabilities. Another difficulty is to design detectors that are fully insensitive to tiny beam displacements.

2. Experimental

Since a complete layout of the ESRF beamline ID12A is presented elsewhere in the same issue (Goulon *et al.*, 1998), together with a discussion of the performances of the optical components of the beamline, we will concentrate here only on the characteristics of the source and on the gap-scan procedure. Note that all spectra reproduced in the following section were recorded by monitoring the fluorescence (FY) of the sample as a function of the energy of the incident photons. All fluorescence detectors, intensity monitors or position monitors installed at beamline ID12A are (single- or multi-anode) silicon photodiodes associated with digital lock-ins exploiting a square-wave-modulated X-ray beam (Gauthier *et al.*, 1995).

2.1. Helios-II undulator source

The source most commonly used at the ESRF beamline ID12A is the helical undulator Helios-II which has 31 magnetic periods (Elleaume, 1994). Horizontal (B_x) and vertical (B_z) magnetic field distributions featuring the same spatial periodicity ($\lambda_u = 52$ mm) are generated by two planar arrays of permanent magnets assembled in two magnetic jaws fixed to rigid girders. The users have access to three independent translations: an axial translation (T_y) of the upper girder induces a variation of the ‘phase’ (φ) between the horizontal and vertical fields and is commonly used to select right-handed ($\varphi = \pi/2$; $T_y = \lambda_u/4$), left-handed ($\varphi = -\pi/2$; $T_y = -\lambda_u/4$) or linear ($\varphi = 0$; $T_y = 0$) polarizations; vertical translations (T_z) of each individual girder are used not only to shift the undulator peak energy but also to vary the ratio $\rho = B_x/B_z$, which is critical to maximize the circular polarization rate ($\rho = 1$). Note that for elliptical polarizations ($\rho \neq 1$), varying ρ will rotate the long axis, change the ellipticity and modify the relative intensities of high-order harmonics (Elleaume *et al.*, 1991). A critical adjustment of the two half-gaps is thus quite essential. For any undulator setting, the field integral can be kept below $30 \mu\text{Tm}$ thanks to a very efficient multipole shimming technique (Chavanne *et al.*, 1992).

2.2. Undulator gap-scan procedure

One needs first to build up a lock-up table which correlates (for any desired polarization state) the displacements $T_z(B_x)$ and $T_z(B_z)$, or the corresponding ‘half-gaps’ values, with the energy of the maximum of the undulator peak. Let us start with the simplest case where only one half-gap is varied during an energy scan. We use a second-order polynomial fit of the data stored in the lock-up table to calculate the optimized values of the translation $T_z(B_x)$ or $T_z(B_z)$ for any energy (or Bragg angle) of the

monochromator. A flow chart (Fig. 1) summarizes the whole procedure programmed under *SPEC* (Certified Scientific Software, Cambridge, MA, USA): the input parameters include the values of A , B and C (fitted from the data stored in the lock-up table), the starting (E_{\min}) and final (E_{\max}) energies of the scan and the number of data points (N_{pts}). For every energy, the optimized gap is calculated and is compared with the previous setting. If the difference exceeds $2.5 \mu\text{m}$ (minimum step size authorized) then the gap is moved to its optimum value. Depending on the absolute half-gap settings, the undulator peak may shift by 2–5 eV.

Moving only one single half-gap is not acceptable for circular dichroism experiments since the ellipticity of the X-ray beam would change during the scan. A modified procedure (hereafter called ‘double’ gap-scan) has thus been elaborated where both half-gaps are changed simultaneously in a correlated way according to the equation

$$[\text{half-gap } B_z] = 1.7641 + 1.2489 \times [\text{half-gap } B_x], \quad (1)$$

so that the horizontal and vertical magnetic fields are kept strictly equal ($\rho = 1$).

3. Results

3.1. Sulfur K -edge EXAFS of $[d,l]$ cystine

In the perspective of further EXAFS studies on low- Z elements, we tried first to evaluate the performances of the ‘gap-scan’ technique by recording the EXAFS spectrum of a pellet of $[d,l]$ cystine at the sulfur K -edge. This was a rather demanding test because (i) the EXAFS signal is expected to be very weak (especially at room temperature) since this compound has a very low symmetry, and (ii) high-quality data over a large energy range are required to have a chance of resolving the close-lying $S \cdots C$ and $S \cdots S$ signatures expected at 1.8 and 2.03 Å, respectively. For this experiment, the half-gap B_x was completely open so that the undulator radiation was linearly polarized with the polarization vector in the horizontal plane. The only chance to

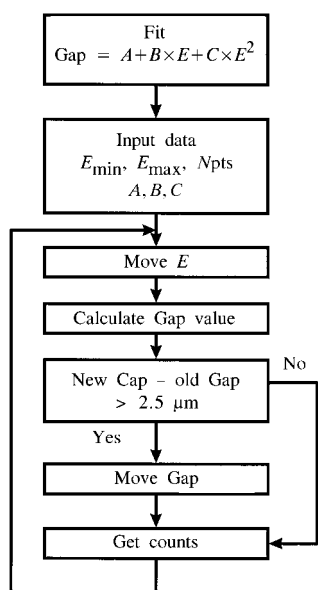


Figure 1
Flow chart of the gap-scan procedure.

record an EXAFS spectrum over a wide energy range (*i.e.* 2400–3800 eV) was therefore by scanning the half-gap B_z . As illustrated by Fig. 2(a), the EXAFS oscillations $k\chi(k)$ clearly extend over more than 18 \AA^{-1} with still a very high signal-to-noise ratio, while the experimental cut-off of earlier data recorded at the sulfur K -edge hardly exceeded 10 or 12 \AA^{-1} . We have reproduced in Fig. 2(b) the Fourier-transformed spectrum corrected for the phase shifts and the backscattering amplitude of the $[S_1 \cdots C_{1\gamma}]$ absorber–scatterer pair. Note that the signatures of the first two shells are well resolved and that the first few interatomic distances [$R_1(S_1^* - C_{1\gamma}) = 1.8$, $R_2(S_1^* - S_2) = 2.03$, $R_3(S_1^* - C_{2\beta}) = 2.84$ and $R_4(S_2^* - C_{1\gamma}) = 3.03 \text{ \AA}$] agree perfectly with the crystal structure data (Chaney & Steinrauf, 1974).

3.2. Spin-polarized EXAFS spectra of EuS at the Eu L -edges

The ‘double’ gap-scan technique was used to record spin-polarized EXAFS spectra over a wide energy range encompassing both the L_{II} - and L_{III} -edges of rare-earth absorbers: here the key advantage is that the polarization rate of the X-ray photons can be kept almost constant over the whole energy range so that the signatures measured at both edges can be directly compared without correction. Ferromagnetic EuS ($T_C = 16.3 \text{ K}$) was selected as a test compound since it was known to exhibit a quite intense X-ray magnetic circular dichroism (X-MCD) signal at the Eu L -edges (Rogalev *et al.*, 1997). The sample (*i.e.* a pellet of EuS diluted in BN) was mounted onto the cold finger of a liquid-helium cryostat ($T = 2 \text{ K}$) located between the poles of a

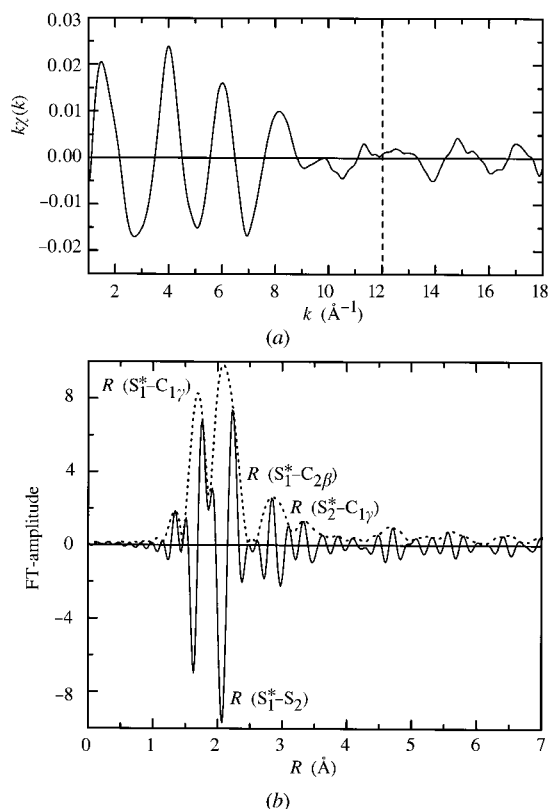


Figure 2
(a) Normalized $k\chi(k)$ EXAFS spectrum of $[d,l]$ cystine recorded at the sulfur K -edge. The dotted line at 12 \AA^{-1} refers to the typical cut-off of earlier data at the sulfur K -edge. (b) FT-EXAFS spectrum of $[d,l]$ cystine corrected for the phase shifts and backscattering amplitude of the $S_1 \cdots C_{1\gamma}$ pair.

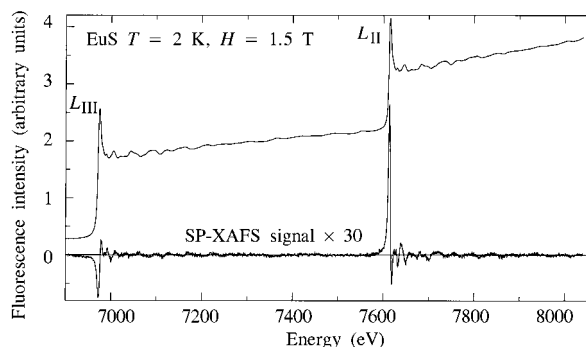


Figure 3

Spin-averaged and spin-polarized XAFS spectra of EuS at the Eu $L_{II,III}$ edges in the ferromagnetic phase. The SP-XAFS spectrum is a direct difference of two consecutive scans recorded with opposite photon helicity.

superconducting electromagnet ($B = 1.5$ T). We have reproduced in Fig. 3 the spin-polarized differential EXAFS spectrum, *i.e.* the difference between two consecutive spectra recorded with opposite helicities of the incident X-ray photons, and the spin-averaged EXAFS spectrum. The data were collected over more than 1000 eV on readjusting simultaneously the half-gaps B_x and B_z . A detailed analysis of these experiments is to be published elsewhere (Rogalev *et al.*, 1998). In the latter spin-polarized difference spectrum, there is no perceptible discontinuity that might be correlated to a gap change, even on the scale of tiny spin-polarized EXAFS signatures. We would also like to mention that strictly the same gap scan has been repeated on replacing the sample by a beam-position monitor (Gauthier *et al.*, 1995): we failed to detect any displacement greater than $5 \mu\text{m}$ of the baricentric location of the monochromatic X-ray beam during a change of gap.

4. Conclusions

Two 'gap-scan' procedures are available: (i) the standard procedure keeps the undulator permanently tuned to its peak intensity during an EXAFS scan and may be used either with planar or helical undulators; (ii) in the case of helical undulators of the Helios type, the 'double gap-scan' technique also keeps the polarization rate almost constant over a wide energy range. As reflected by the excellent quality of the spectra produced in Fig. 2 and Fig. 3, both techniques were found to be perfectly reliable.

We are grateful to A. Götz, J. Klora and V. Rey Bakaikoa for their help in developing and debugging the gap-scan software.

References

- Chaney, M. O. & Steinrauf, L. K. (1974). *Acta Cryst.* **B30**, 711–716.
- Chavanne, J., Chinchio, E., Diot, M., Elleaume, P., Frachon, D., Marechal, X., Mariaggi, C. & Revol, F. (1992). *Rev. Sci. Instrum.* **63**(1), 317–320.
- Elleaume, P. (1994). *J. Synchrotron Rad.* **1**, 19–26.
- Elleaume, P., Chavanne, J., Marechal, X., Goulon, J., Braicovich, L., Malgrange, C., Emerich, H., Marot, G. & Susini, J. (1991). *Nucl. Instrum. Methods*, **A308**, 382–389.
- Gauthier, C., Goujon, G., Feite, S., Moguiline, E., Braicovich, L., Brookes, N. B. & Goulon, J. (1995). *Physica*, **B208/209**, 232–234.
- Goulon, J., Rogalev, A., Gauthier, C., Goulon-Ginet, C., Paste, S., Signorato, R., Neumann, C., Varga, L. & Malgrange, C. (1998). *J. Synchrotron Rad.* **5**, 232–238.
- Hagelstein, M., San Miguel, A., Fontaine, A. & Goulon, J. (1997). *J. Phys. IV*, **7**(C2), 303–308.
- Rogalev, A., Goedkoop, J. B., Rogaleva, M., Gotte, V. & Goulon, J. (1997). *J. Phys. IV*, **7**(C2), 465–466.
- Rogalev, A., Neumann, C., Gotte, V. & Goulon, J. (1998). *Phys. Rev. Lett.* Submitted.